Building-integrated photovoltaics

An investigation of solar modules as ventilated curtain wall facade depending on the specific rear-ventilation and insulation

Masterthesis

in the course of studies
Renewable Energies

Faculty 1
School of Engineering – Energy and Information

at the
Hochschule für Technik und Wirtschaft Berlin

submitted by
Niklas Albinius

Berlin, 14.04.2022

First Supervisor: Prof. Dr. Rutger Schlatmann
Second Supervisor: Dr. Carolin Ulbrich

I. Table of contents

II. List of figures

IV. List of abbreviations [1]

abZ	allgemeine bauaufsichtliche Zulassung (*general technical building approval*)
AC	Alternating current
BIPV	Building-integrated photovoltaics
DC	Direct current Global
DIBt	Deutsches Institut für Bautechnik *(German Institute for Construction Technology)*
GCB	Generator connection box
GHI	Global horizontal irradiance
GTI	Global tilted irradiance
HZB	Helmholtz-Zentrum Berlin
PV	Photovoltaics

1 Abstract

The concept of building-integrated photovoltaics (BIPV) strives to make more surfaces accessible for solar electricity generation. Especially in urban areas, there is a huge potential in PV facade installations due to the large available facade areas compared to roofs and open fields [2]. The option to integrate PV modules in the entire building envelope brings greater architectural freedom in design at the cost of additional effort in planning and construction. Yet, BIPV is not as common in newly constructed buildings as it could be. In part this is due to the fact that PV modules need to meet a variety of architectural demands. Respectively the installation of the PV modules has its own requirements.

This thesis investigates an architectural aspect in respect to its influence on PV performance. Literature shows, that higher PV module temperatures lower the overall PV performance and module lifetime [1] [3] [4]. Integrated PV modules are usually less well ventilated than modules in a conventional PV system. To enhance the efficiency of BIPV installations, sufficient cooling is key. The lower natural ventilation often needs further support. When integrated as a ventilated curtain wall, PV modules can benefit from additional passive vertical ventilation, which compensates the lack in natural cooling. This thesis analyzes the data acquired at a BIPV facade with intentionally different rear ventilation situation.

In 2021, a new laboratory building with an integrated PV system was constructed by the Helmholtz-Zentrum Berlin (HZB). The 50 kWp facade-integrated PV system replaces a commonly used aluminum facade with light blue CIGS modules. The PV modules, which serve as ventilated curtain wall facade, are installed on the south, west and partly on the north side of the building. The whole system is monitored by a variety of sensors, which provide detailed insight on electrical components, module temperature, ventilation, irradiance, and other local weather conditions.

This investigation compares two different facade substructures and the influence of the resulting difference in rear-ventilation on the PV performance. A 56 m² big facade section allows for a long-term study of the influence of the air velocity on commercial PV modules. In this work, the system was reviewed from the 1st of December 2021 to the 2nd of April 2022.

Surprisingly, even though differences in the measured air velocity and module temperature could be observed in the period under review, no significant influence on the overall PV performance could be shown. This fact implies greater freedom for architects and planners in the process of designing and planning future projects with facade-integrated PV modules.

2   Introduction

2.1   Building-integrated photovoltaics

Part 1 of the EN 50583 standard [5] is providing the following definition for building-integrated photovoltaic modules:

> *"Photovoltaic modules are considered to be building-integrated, if the PV modules form a construction product providing a function as defined in the European Construction Product Regulation CPR 305/2011. Thus, the BIPV module is a prerequisite for the integrity of the building's functionality. If the module is dismounted […], the PV module would have to be replaced by an appropriate construction product."*

Furthermore, this standard aims to specify these building functions. If the PV module fulfils any of the following building functions while replacing a building element, the installation can be classified as BIPV [5].

- Mechanical rigidity or structural integrity
- Primary weather impact protection: rain, snow, wind, hail
- Energy economy, such as shading, daylighting, thermal insulation
- Fire protection
- Noise protection
- Separation between indoor and outdoor environments
- Security, shelter or safety

Besides these building standards, there is currently no uniform definitions to evaluate any case specific PV system in respect to it being building-integrated or not. The Helmholtz-Zentrum Berlin (HZB) states, that according to the applied definition not only elements with constructional features can be replaced, but also elements with purely aesthetic features [6].

Furthermore, the HZB provides a visual overview over different kinds of BIPV solutions. The following picture shows an exemplary single-family home with an attached garage, all covered by different BIPV applications. Important to note is that the usual mounted PV system as depicted on the garage does not qualify as BIPV.
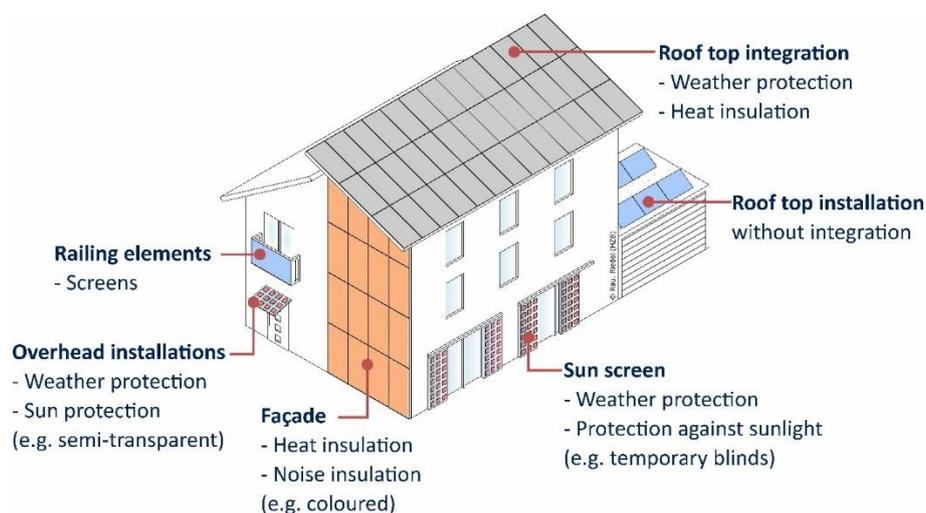
Figure 1: Schematic illustration of the different opportunities to integrate photovoltaics into the building © HZB

2.2   Living Lab for Building-integrated Photovoltaics

In early 2022, the construction of a new laboratory building of the HZB in Berlin Adlershof was finished. The purpose of the building is to give room for physics laboratories, testing facilities, IT infrastructure and clean rooms.

Besides all the facilities on the inside, an important research project is located on the outside. 360 fully integrated thin-film solar modules are part of a BIPV system, which cover a large area of the facade. That is why this new building is called Living Lab for Building-integrated Photovoltaics. The module areas which envelop the facade can be seen in the following Figure 2.

Figure 2: HZB Living Lab for Building-integrated Photovoltaics (South-West view)

These frameless and colored PV modules function as ventilated curtain wall facade with the ability to harvest solar energy. The modules are installed in three different facade orientations: South, West, and North. In the south facade 248 modules are integrated, while the modules integrated in the West and North facade amount to 56 respectively.

The blue solar modules chosen for the integration are Avancis Skala 7003 modules. These thin-film solar modules have a nominal power of 140 Wp with a tolerance of manufacturing of -5 %/+10 %. This comparatively low nominal power is mainly due to the rather small dimensions (1587 mm x 664 mm) and the cell type (copper-indium-gallium-selenide). These modules were chosen for two reasons. Firstly, the visible part of the integrated solar module is a completely frameless, homogeneous glass surface. From greater distance these solar modules are hardly recognizable as such. Secondly, the solar modules are mounted on a back rail system which is compatible with many facade substructures. Because the solar modules are hung into the back rail system, no additional clamps are needed to secure the modules. This aspect is of major importance to facilitate the use of BIPV products for architects, engineers and construction workers.

There is also a practical reason for the choice of modules. The Avancis GmbH is one of the few BIPV module manufacturers, who has a general technical building approval (abZ) from the Deutsches Institut für Bautechnik (DIBt). For any building project which uses building elements without an abZ it is significantly harder and more time-consuming to obtain a building permit in Germany. BIPV modules would need a separate approval for the individual case, which would only be valid for the current project.

This work will only focus on a specific part of this 50 kWp solar system. Although multiple sensors for different measurements are located all over the facade, a large part of them is located on the far-left side of the South oriented facade. There, on the edge of the South and West facade, a variation in the facade substructure has been implemented.

The investigation aims to show to what extent the facade substructure can influence the performance of the integrated solar modules. For this purpose, additional insulating mats were attached to a part of the substructure at the corner of the building in order to increase the insulating effect and to narrow the air gap. Figure 3 shows the boundary layer between both facade substructure variation during the building process. On the left side, the insulation clearly has been thickened by the additional insulation mats.

To further clarify the exact difference in the facade substructure, a schematic compari-

Figure 3: Schematic difference in the facade substructure

son of the variation is depicted in Figure 4. The attachment of the modules as well as the back rail system is shown in a simplified way for clarity. Note, that air flow is possible even between the individual beams of the facade substructure and not just in the right facade variation with an additional air gap between substructure and insulation. The overall air gap in the left substructure variation is 5 cm wide, while the overall air gap in the right substructure variation is 15 cm wide.


Figure 4: Schematic facade cross section of both variations of the module substructure

3   Theoretical basics

3.1   PV power

The electrical power generated by a photovoltaic system, module or cell is called the PV power. A single solar cell is able to generate this electric power by directly converting energy from the sun into a flow of electrons by the photovoltaic effect. If these cells are added together to solar modules which also can be added together to whole solar systems, the generated PV power increases. Depending on the size of a PV system, the amount of generated PV power can supply an entire household or even villages and smaller cities.

The PV power can be calculated by the basic formular of the electrical power. The power of a solar cell equals the current multiplied by the voltage of said cell [4]. Therefore, the PV power increases if one or both parameters increase. Despite of type-dependent differences of the cells, several other factors are having an influence on these parameters.

The solar irradiance has a very high influence on the performance of a PV cell. The intensity of the irradiation is the driving factor which contributes to power generation [4]. A high and non-fluctuating irradiance is therefore highly desirable for the operation of a solar system. The irradiation which hits the solar cell can be decreased by blocking the cells from the sun. This can happen by cloud movement or the casting of shadows from nearby buildings or vegetation. Even a single bird's dropping on top of a solar cell can decrease the PV power by lowering the irradiance on the cell. Additionally, the angle in which the irradiation hits the cell can also influence the power output. Obviously, the most power can be generated when the module is directly facing the sun.

The module temperature not only influences the PV power output but is also a contributing factor to the degradation process [1]. A high module temperature increases the short circuit current slightly but lowers the open-circuit voltage drastically. Therefore, the overall power decreases. This phenomenon is usually quantified with the temperature coefficient in the data sheets of the used PV module. Typical temperature coefficient for CIGS modules range from -0,35 %/°C to -0,5 %/°C [4]. That is why, proper cooling is crucial to minimize this effect on the generated PV power output.

Despite the losses which are mostly caused by external influences, there are other losses caused by additional electrical components of the PV system. Every cable and every monitoring device has minor losses. Furthermore, power is also lost during the current conversion.

The flow of charge from a PV system moves only in one direction. A PV system generates so called DC power, which refers to the **d**irect **c**urrent, which often has to be converted for usage. Most household items and the electricity grid in Germany operate on so called AC power, which uses the **a**lternating **c**urrent. The electric charge of an alternating current changes periodically. To convert the generated DC power from a PV system to the more commonly needed AC power, a DC/AC inverter is needed. These inverters can change the direction of the flow of charge at the price of a small thermal energy loss. The efficiencies of typical inverter products often surpass 90 % by far [4].

The amount of generated PV power is the main indicator of the performance of a PV system. System operators strive to maximize the energy yield by assuring that their system is properly ventilated and advantageously placed for the best capture of solar irradiation. A comparison of the generated PV power is commonly used method to evaluate different PV systems. In the case of the investigated BIPV system, both facade substructures will also be compared by the amount of generated PV power. A higher PV power output on one side of the facade, indicates which facade substructure is more suitable to use with an integrated PV system.

3.2   Module temperature

As stated in the previous chapter 3.1, the temperature of a PV module not only has influence on the degradation of the module but also can cause a severe loss in power. Several factors have an influence on the module temperature, first and foremost the solar irradiation. An increase in temperature of the solar module during the operation cannot be prevented. The intensity of the increase can be reduced by assuring proper cooling and ventilation of the modules.

If not measured, the module temperature T_{mod} can be estimated using the following simple linear expression [3]:

$$T_{mod} = T_{amb} + k \cdot G$$

Within this expression, the module temperature is approached by adding the ambient temperature T_{amb} to the incident solar irradiation G multiplied by the Ross coefficient k. This Ross coefficient varies from 0,02 to 0,06 K m²/W depending on several different aspects like the cell type, ambient wind velocity and other characteristics of the system. Even though precise values can be found in literature, they are dispersed depending on these characteristics [3].

The module temperature of the investigated PV system gets measured on the rear side of the installed modules. Therefore, a calculation won't be necessary. Nevertheless, the calculation approach shows the key parameters which influence the module temperature. Even though the ambient wind speed on the air flow velocity of the rear-ventilation might influence the Ross coefficient and therefore the module temperature, the ambient temperature and the solar irradiation have a much higher impact.

3.3   Air flow velocity

To quantify the rear-ventilation of the investigated BIPV system, the air flow velocity is measured. As stated in the previous chapter 3.2, the temperature of the solar modules increases under operation. A high module temperature is not desirable, that is why proper cooling should be provided.

The rear-ventilation of a ventilated curtain wall facade has to fulfil certain tasks to prevent heat loss of the building or damage to the building elements. Regarding the BIPV system only a proper dissipation of the rising module temperature is important. Therefore, the heat transfer via convection is the most important factor to consider. The convective heat transfer $\dot{Q}_C$ can be calculated as follows [7]:

$$\dot{Q}_C = h \cdot A_S \cdot (T_f - T_s)$$

where A_S is the surface area of the cooled object, T_s the surface temperature of the cooled object, T_f the fluid temperature, b a scaling exponent, and h the heat transfer coefficient. This coefficient is highly dependent on multiple different factors, such as the type of flow, the heat flux, the fluid viscosity, or the fluid velocity. This coefficient has been recorded empirically for commonly encountered scenarios [6]. Note, that the flow rate has no influence on said coefficient [8]. That is why, in order to evaluate the amount of transferred heat the focus will lie on the air velocity. Other parameters, which in influence this coefficient, do not differ between both substructure variations.

Facade integrated PV modules are not solely cooled by the ventilation on their rear side. Convective heat transfer also happens at the module front, because of ambient winds. It is to be expected, that the modules can be better cooled by the ambient winds because these show a much higher air flow velocity which then lets the heat dissipated faster.

4 Experimental basics

4.1 Measuring devices

Three of the installed sensor types are of primary importance to the investigation in hand. Digital thermometers are used to determine the module rear temperature. Additional string monitoring devices provide insight into the electrical behavior of each individual string. Air flow sensors determine the air velocity behind the modules to show possible differences in the ventilation. In the following, these three sensors will be examined in more detail.

Digital thermometer

The module rear temperature is measured by the DS18B20 digital thermometer from the Maxim Integrated Products Inc. on multiple solar modules. The whole PV system is equipped with 72 temperature sensors. The area under investigation is monitored by 18 of these.

The used thermometer is a silicon bandgap temperature sensor. The advantages of this type of sensor are a fast and accurate response, the overall small size, and the rather low cost. Most importantly, the temperature signal is directly converted into an electric signal, which can easily be digitally monitored.

The temperature sensor has an operating temperature range of -55°C to +125°C. While the measured temperatures lie in range of -10°C to +85°C the accuracy of the measurement is ±0,5%. This corridor was only left on rare occasions in winter during nighttime, where the ambient temperature drops below -10°C. During regular daytime measurements, the temperature always stayed within range.

The temperature sensor is glued to the rear side of the module with a heat conductive adhesive. The sensor is also covered by a protective layer of an adhesive tape to secure its position on the module even further. The taped down sensors are highlighted by a red circle in Figure 5. A highly desired feature of these sensors is the connection to the temperature logger via a single cable. Less cables and otherwise dangling parts ensure a proper air flow behind the solar modules.

Figure 5: Temperature sensors on the solar module rear side (circled in red)

The module rear temperature is only measured on certain parts of the facade, just like in the area under investigation. Not every single module is temperature monitored. Only selected modules in proper distance to each other are equipped with a sensor to ensure maximum coverage of the area while using a small number of sensors. Some modules are equipped with two temperature sensors to show the difference between the center and edge temperature. The precise placement of each sensor is later shown in Figure 10.

String monitoring device

Each solar module is connected with other solar modules to so called strings. These strings are individually monitored by string monitoring devices (shown in Figure 6). These have to be integrated into the generator connection boxes (GCB), to provide sufficient protection for the electronics. A string monitoring device integrated in a GCB can be seen in Figure 7.

Figure 6: Kernel ST2 0825 string monitoring device

Two different string monitoring devices are used for the PV system. That is why it is important to note, which one is used for which string. There are eight Raycap ProSMS8 devices and three Kernel ST2 0825 devices in use. In the following, the specifications of the Kernel devices will be discussed since this work focuses on a specific part of the facade where only Kernel devices are used. When a string monitoring device is mentioned later, it refers to the Kernel product.

Each Kernel device is connected with five strings of seven solar modules. Since the area under investigation has 56 modules, two string monitoring devices are needed to monitor the area. Since the string monitoring devices measure current and voltage before the inverters convert the direct current to alternating current, the calculated PV power differs from the analytics software of the inverters. It is important to keep in mind, that even though both measurements record the PV power of the same system, the inverters got a 98% efficiency for the current conversion. A small loss in power must be expected, which is why the inverters should measure a lower PV power.

The data from each individual string monitoring device is getting read by a python script. The script circles through every Kernel device and collects the measured data in a .csv-file every 3 minutes. Because the process of reading, saving, and circling to the next device takes a short amount of time, the measurements don't exactly happen every 3 minutes. A small shift of 3 to 6 seconds between each measurement can be observed.

The measurement via the string monitoring devices has been unstable since installation. Certain settings have caused the system to shut down at particularly low irradiation levels. Due to these irregular shutdowns some of the measured data sets have become unusable, which happened especially in the early operation of the system. Solutions and workarounds are still being worked on to this day, to eliminate these problems one after another.

One of these workarounds is necessary for the daily boot-up of the measurement system. If the measurement system has not already booted by itself, it is started at 9:00 am by a separate script. At this time the irradiation is usually already high enough so that the system does not shut down again directly. If the irradiation is too low, the minimum electrical limits of the system are undercut. Required is a minimum voltage of 100 V and a minimum current of 1 A. That's why as soon as the string power falls below 0.1 kW for a longer period of time, the measuring system shuts down.
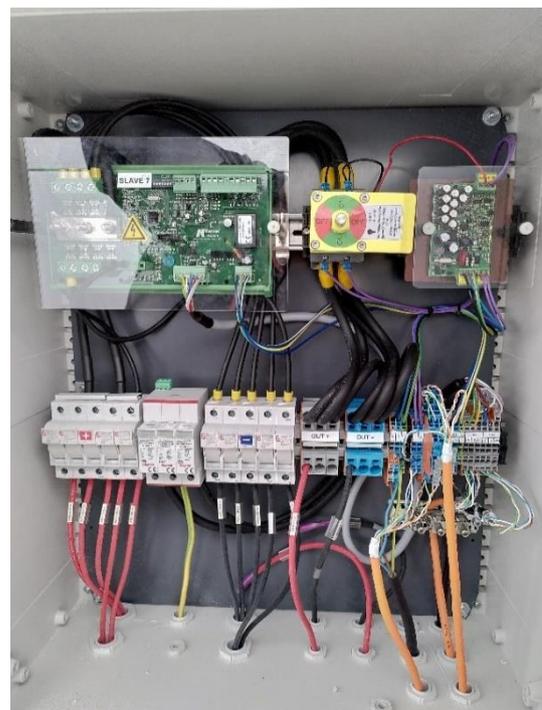
Figure 7: GCB with integrated Kernel device

Air flow sensor

To quantify the rear-ventilation behind the solar modules, four air flow sensor are installed into the air gap. For this purpose, the SCHMIDT® Flow Sensor SS 20.500 has been chosen. This sensor can precisely measure the velocity of an air flow, even if the air is polluted by dust or various gases. The air gap behind the modules is not fully closed off to small particles or insects which is why some pollution has to be expected. As shown in Figure 8, the device gets attached to the module substructure and aligned so that the air flow hits the sensor in an orthogonal angle.

Figure 8: Placement of the air flow measurement device during the construction process

The sensor of the measurement device does not measure the velocity of the air flow but a change in power of a heater. On the tip of the measurement device between the so called "dumbbell disks" the temperature sensor is getting heated up 40 K above the additional measured medium temperature. The exact location of the sensor is highlighted in Figure 9. The electrical power which is necessary to maintain this temperature difference between the medium and the sensor is the key measurement, which is required to calculate the velocity of the air flow. Therefore, the air flow velocity recorded by the sensor isn't actually measured but calculated. The datasheet of the device states, that the value of the air velocity has an accuracy of ±3%.
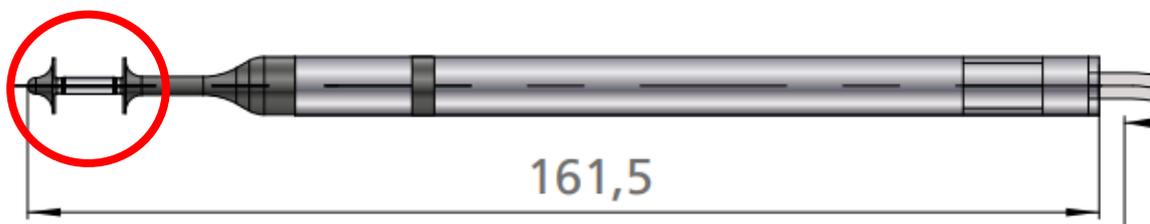
Figure 9: Schematic image of the air flow measuring device with the circled temperature sensor

Every measurement of this device before the 15th of April 2022 has a small, but unknown shift on the time axis. Due to unexpected shutdowns of the device, the timestamp of each measurement can have an up to 10 min inaccuracy. Since that day, the measurement is synchronized with a time server. That's why all used ventilation data was measured after this day.

4.2   Measurement uncertainties and possible errors

As already shown in chapter 4.1, each measuring device inherits a measurement accuracy. An error propagation calculation has to be done, if these measurements are further used in other calculations. The formulars used in the following are taken from several sources of fundamental literature [9] [10] [11].

Since the module rear temperature and the ambient temperature will are used in further calculations, the given uncertainty cannot be directly applied while analyzing the figures. Each measured module rear temperature has an accuracy of ±0,5 % and the ambient temperature an accuracy of ±0,4 %. Since an average module temperature gets calculated, an error calculation must be done.

The measurement of the global horizontal irradiance (GHI) and global tilted irradiance (GTI) will neither be used for further calculations. That is why, no error propagation must be calculated. Since the accuracy of an irradiation measurement is multi-layered and complex, the ISO 9060 standard [12] aims to classify these for comparability. The GHI is measured by a thermal pyranometer of Class A while the GTI is measured by a silicon pyranometer of class C.

The air flow velocity and the ambient wind speed measurement suffer from severe fluctuations, which make their graphs unreadable. Therefore, an average gets applied to smoothen out the courses and make differences clearer. Since the original values were used in a calculation, an error calculation must be done too. The former relative error of the air flow velocity is ±3 %.

The arithmetic mean average is calculated by the sum of values divided be the number of values N:

$$\bar{x} = \frac{1}{N} \cdot \sum_i x_i$$

The error Δx of the arithmetic mean average is calculated by:

$$\Delta x = \frac{1}{N} \cdot \sqrt{\sum_i x_i^2} = \frac{1}{\sqrt{N}} \cdot \sqrt{\frac{1}{N} \cdot \sum_i \Delta x_i^2}$$

If every single measurement error is the same, the previous formular can be simplified to:

$$\Delta x = \frac{1}{\sqrt{N}} \cdot \Delta x_i$$

The average string temperature is calculated from different numbers of measurements. Some modules are equipped with a center and an edge sensor, which doubles the number of measurements considered. Since the same measurement device was used for each measurement, every single measurement error is identical. Therefore, the simplified formular can be used and the two different errors of the arithmetic mean average of the module rear temperature will amount to:

$$\Delta T_{3S} = \frac{1}{\sqrt{3}} \cdot \pm 0{,}5\% \approx \pm 0{,}29\%$$

$$\Delta T_{6S} = \frac{1}{\sqrt{6}} \cdot \pm 0{,}5\% \approx \pm 0{,}20\%$$

The used moving average for the air flow is calculated by a window size of 180. Since every air velocity measurement is also taken by the same devices, the accuracy of the average air velocity can be calculated with the same formular and amounts to:

$$\Delta v = \frac{1}{\sqrt{180}} \cdot \pm 3\% \approx \pm 0{,}22\%$$

The same calculation is applied to the ambient wind speed which is measured by the weather station on the roof of the investigated laboratory building. For the build-in anemometer no measurement accuracy has been listed in the respective data sheet. If an exceptionally high measurement error of 10% for each measurement is assumed, the overall relative error of the average ambient wind speed would still not rise above ±1%.

The uncertainty of the PV power must also be calculated from the measurement accuracy of the string monitoring devices. Current and Voltage each show an individual measurement accuracy. Because the PV power is not measured directly, the measurement accuracy must also be calculated. The current reading accuracy is listed with an error of 0,15% in the respective datasheet provided by the Kernel. The voltage reading accuracy has not been listed in this datasheet and wasn't provided by Kernel even when asked. To be able to estimate the relative error for the PV power, the voltage error of 0,5% from the Raycap device is assumed here.

To quantify a sufficient relative error for the PV power, the maximum absolute error ΔE_{max} must be calculated first by using the following formulars:

$$\Delta E(x_1, \dots, x_n)_{max} = \sum_{i=1}^{n} \left| \frac{\partial}{\partial x_i} \cdot E(\bar{x}_1, \dots, \bar{x}_n) \cdot \Delta x_i \right|$$

The measurement errors for the current ΔI and the voltage ΔU can be directly taken from the data sheets and inserted into the formula. Therefore, the maximum absolute error of the PV power ΔP_{max} is calculated by:

$$\Delta P(I, U)_{max} = \left| \frac{\partial}{\partial I} P(\bar{I}, \bar{U}) \cdot \Delta I \right| + \left| \frac{\partial}{\partial U} P(\bar{I}, \bar{U}) \cdot \Delta U \right|$$

$$= \left| \frac{\partial}{\partial I} P(\bar{I}, \bar{U}) \cdot I \cdot 0{,}0015 \right| + \left| \frac{\partial}{\partial U} P(\bar{I}, \bar{U}) \cdot U \cdot 0{,}005 \right|$$

The maximum relative error δE_{max} is calculated by:

$$\delta E_{max} = \frac{\Delta E_{max}}{|\bar{x}|}$$

To calculate the maximum relative error of the PV power δP_{max}, the previous calculated maximum absolute error must be inserted in the formular.

$$\delta P_{max} = \frac{\Delta P_{max}}{|\bar{P}|}$$

Since the maximum error does not always occur, an average error can be more suitable to describe the measurement uncertainties [11]. The average absolute error $\Delta\bar{E}$ is calculated by:

$$\Delta\bar{E}(\bar{x}_1, \dots , \bar{x}_n) = \sqrt{\sum_{i=1}^{n}\left(\frac{\partial}{\partial x_i} \cdot E(\bar{x}_1, \dots , \bar{x}_n) \cdot \Delta x_i\right)^2}$$

Again, the measurement errors for the current ΔI and the voltage ΔU are taken from the data sheets. Therefore, the average absolute error of the PV power $\Delta\bar{P}$ can be calculated as:

$$\Delta\bar{P} = \sqrt{\left(\frac{\partial}{\partial I}P(\bar{I},\bar{U}) \cdot \Delta I\right)^2 + \left(\frac{\partial}{\partial U}P(\bar{I},\bar{U}) \cdot \Delta U\right)^2}$$

$$= \sqrt{\left(\frac{\partial}{\partial I}P(\bar{I},\bar{U}) \cdot I \cdot 0{,}0015\right)^2 + \left(\frac{\partial}{\partial U}P(\bar{I},\bar{U}) \cdot U \cdot 0{,}005\right)^2}$$

The average relative error $\delta\bar{E}$ is calculated by:

$$\delta\bar{E} = \frac{\Delta\bar{E}}{|x|}$$

To calculate the average relative error of the PV power $\delta\bar{P}$, the previous calculated average absolute error must be inserted in the formular.

$$\delta\bar{P} = \frac{\Delta\bar{P}}{|\bar{P}|}$$

After multiple exemplary insertion of measured data, the value for the maximum and average relative error of the PV power could be safely determined as:

$$\delta P_{max} = 0{,}3\,\%$$
$$\delta\bar{P} \approx 0{,}212\,\%$$

For the following figures of the air flow and module temperature, a relative error has been provided. The evaluation of the depicted data of the PV power will be based on the calculated average relative error.

4.3   Positioning of measurement sensors

The following Figure 10 shows the placement of every single sensor for the measurement in the area under investigation. The green border marks the area under investigation. At the left side where the solar modules are marked in a darker shade of blue, the air gap between the solar modules and the insulation has a width of 5 cm. The right side with the lighter colored solar modules has an air gap width of 15 cm. The small red dots indicate the placement of the temperature sensors, while the big blue dots indicate the placement of the ventilation sensors. The yellow sensors, which were installed to measure the global tilted solar irradiance have most of the time been out of order. An unknown problem caused a data loss of several month during the investigation.
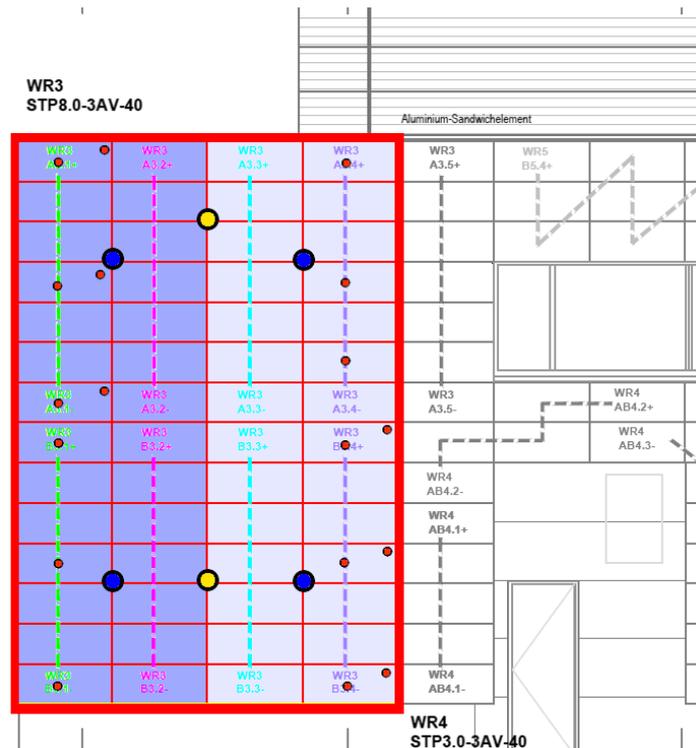

Figure 10: Sensor placement in the area under investigation

At second glance can be observed that no temperature sensors were installed behind the module strings in the middle. All sensors have been placed either on the far left or right side of the area under investigation. Edge effects were expected to take place at the boundary layer between both facade substructures. Since these effects would not exist on a normal homogenous build facade, no investigation is required there.

4.4   Analysis and evaluation methods

The measured data from each measurement device has to be transferred to a central computer for further investigation and evaluation. There, a Python scripts reads the measured data and saves it periodically into single files. Since the measurement intervals, the overall measured parameters and the label of said parameters differ strongly between each measurement device, these files cannot easily be merged. For this reason, another Python script written by the author[1] of this work is used to visualize the measurement of certain parameters. Each data set gets imported and formatted, so that it can be used for further calculations. Multiple figures are created by the script to easily evaluate the measured data visually. Plotly's Python graphing library was chosen to create these figures which in the following will be used for analyzing and evaluation.

---

[1] *This Python script can be provided by the author upon request.*

5   Data analysis

5.1   PV power

Since the inverters cannot portray string specific differences, the measurement by the additional string monitoring devices is used for the analysis of the PV power. Every following depiction of PV power refers to the DC power measured with these string monitoring devices. The following Figure 1Figure 11 shows a comparison of the overall power from the complete PV system and the generated power from the area under investigation on an overall sunny day.
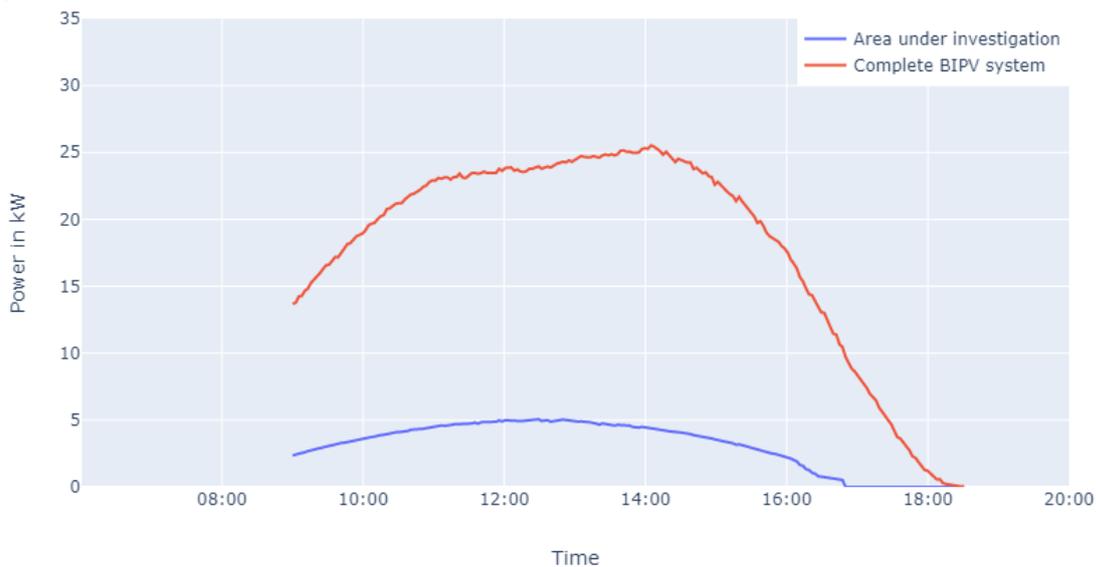

Figure 11: Comparison of data from the AC and DC measurement devices on the 24th of March

As already mentioned in 4.1, the measurement of the string monitoring devices does not start before 9:00 a.m. in the morning. After the measurements have started, a different course is observed. Most noticeable is the overall difference in power. Since the area under investigation is only a small part of the complete BIPV system, the generated power in this area is also only a fraction of the total PV power.

Furthermore, both curves differ in shape. While the generated power in the area under investigation shows a gentle slope with a clear peak during noon, the generated power of the complete BIPV system nearly shows a plateau at the same time. The total power of the system also shows a much steeper slope during morning and evening hours. Additionally, the complete system generates much longer power than the area under investigation. The complete system generates PV power for almost an hour longer after the generated power from the area under investigation can no longer be measured.

To determine the origin of the shape of the curve for the area under investigation in Figure 11, the following Figure 12 and Figure 13 show the influence of higher solar irradiation on a sunny day und lower solar irradiation on a cloudy day. Since the PV power is a function of the irradiance, a high similarity in shape is expected.
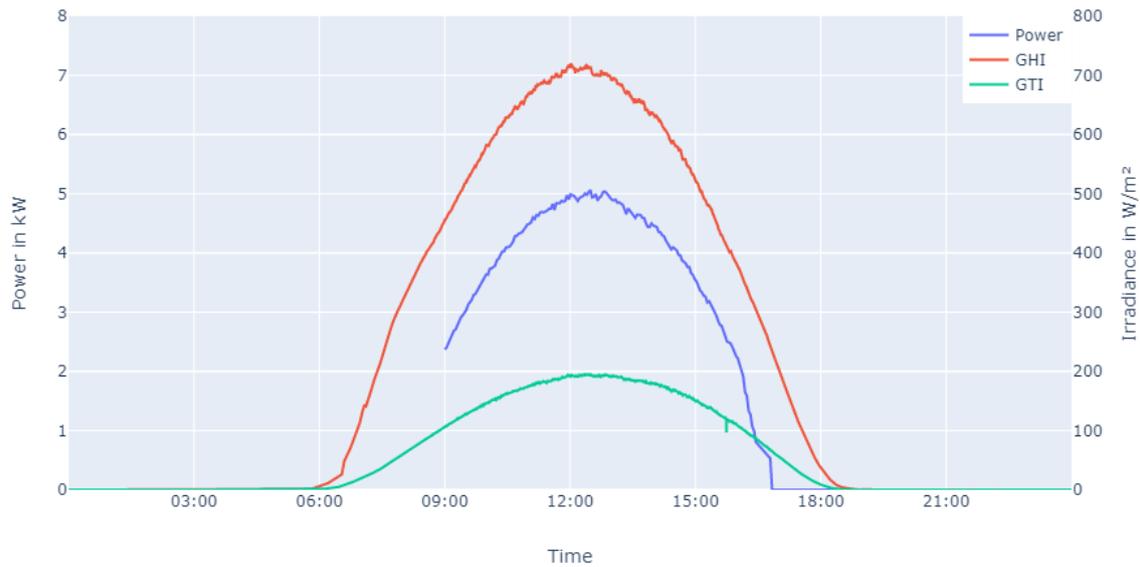
Figure 12: Total PV power in the area under investigation in contrast to the irradiance on the 24th of March

The generated PV power from the area under investigation shows a similar course to the depicted irradiances. However, the smaller fluctuations of the PV power do not pair with the fluctuations of the depicted irradiances. The same behavior is observed during a cloudy day. Figure 13 shows such a day with lots of clouds and high fluctuations in the global horizontal irradiation. These high fluctuations cannot be found in the course of the measured PV power.
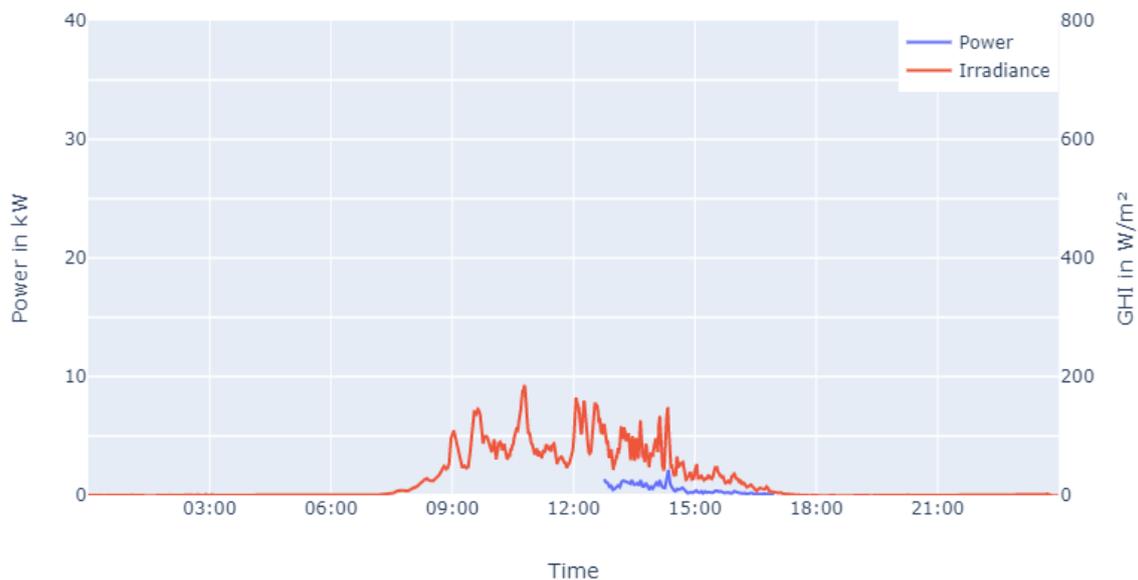

Figure 13: Total PV power in the area under investigation in contrast to the irradiance on the 16th of February

This especially low and fluctuating irradiance shows a common problem of the current setup of the measuring system. A string power of below 100 W cannot be measured and if no measurement can be taken, the measuring protocol shuts down. Although it is possible, that the measurement starts automatically when the generated power surpasses this threshold value, a significant part of the measurement is often lost.

The comparison of Figure 12 and Figure 13 clearly shows the dependency of the PV power from the irradiance. As already mentioned in chapter 3.1, the irradiance has the highest impact on the overall generated PV power, although other parameters can act beneficial or hindering towards it. The observed minor fluctuations in the PV power output cannot solely be attributed to the irradiance.

To find a possible cause of the fluctuations, the PV power got investigated even further. The following Figure 14 shows the generated PV power generated by each single string in the area under investigation. The figure is divided in two parts which show a close-up of the generated power during noon (Part A) and during the afternoon (Part B).
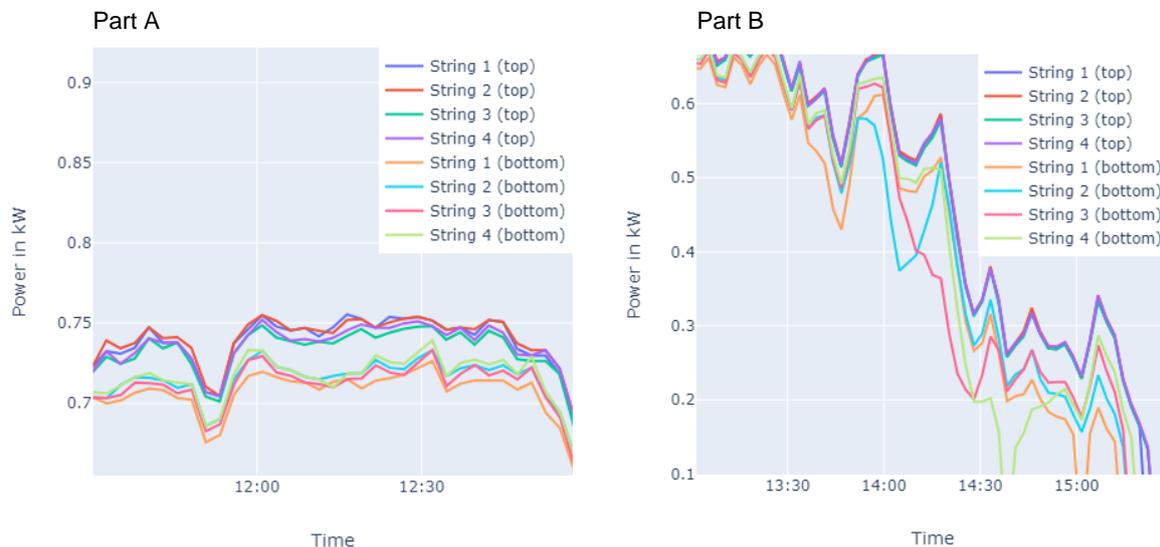

Figure 14: PV power in the area under investigation for each string on the 13th of February

On the 13th of February, rather high fluctuations can be observed evening hours. Especially the bottom half strings are highly fluctuating. During the power peak at noon a rather stable course of all curves can be observed. Interesting is the fact, that every top string consistently performs better than the bottom half strings. Only on rare occasions the bottom strings surpass the top strings in the amount of generated PV power. This excludes the hypothesis, that an offset in the measurement system caused this difference.

Particularly noticeable is the course of the bottom half strings in the evening. Looking at the negative peaks starting at 1:45 p.m., a pattern can be discovered. At first, a drop in the far-left string is shown. A couple minutes later, the string next to it drops in power. These drops in power move from left to right over all four strings. After that, the process seems to start again until no power gets generated any-more. A similar course can be observed during morning hours.

This phenomenon can be attributed to partial shading of the area under investi-gation. As shown in Figure 15 and Figure 33 in the appendix, a nearby group of

Figure 15: Tree shadow over the area under investigation

trees is casting shadows during certain times of the day. The shadow moves over the lowest module of each string and therefore lowers the whole string power. Especially during winter month, where the angle of the sun is much lower, this phenomenon can clearly be observed. As the year progresses and the angle of the sun increases, the shadow is getting shorter and shorter until it only reaches the modules on the far left. An impact on the PV power could be observed at all times in the period under review.

5.2   Module temperature

During the investigation of the module rear temperature high differences in the center and edge measurement were observed on single modules. The temperature difference was still noticeable during nighttime, where no temperature difference should have been observed. After further investigation, these sensors were labeled as defective and were no longer used in any calculation or analysis. A figure which shows this incorrect temperature difference can be found in the appendix.

To get a more general overview of the area under investigation, a temperature average for each module string was formed. That way, the temperature is much more comparable to the air velocity of the rear-ventilation. To further enhance the visual comparability, the area under investigation is divided into 4 equal sections for the following analysis. A color code is applied to each of those section as shown in Figure 16 on the right. Measurement of the bottom right area are colored blue, measurements of the bottom left area are colored red, measurements of the top right area are colored green, and measurements of the top left area are colored purple. This color code is applied for upcoming figures which show

Figure 16: Color code

measurements of the module rear temperature and the air velocity of the rear-ventilation.
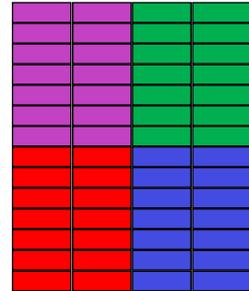
To visualize the effect of high solar irradiance on the module temperature, the following Figure 17 shows the average string temperature of each investigated string with a relative error of ±0,2 %. On the second y-axis the global tilted irradiance shown.
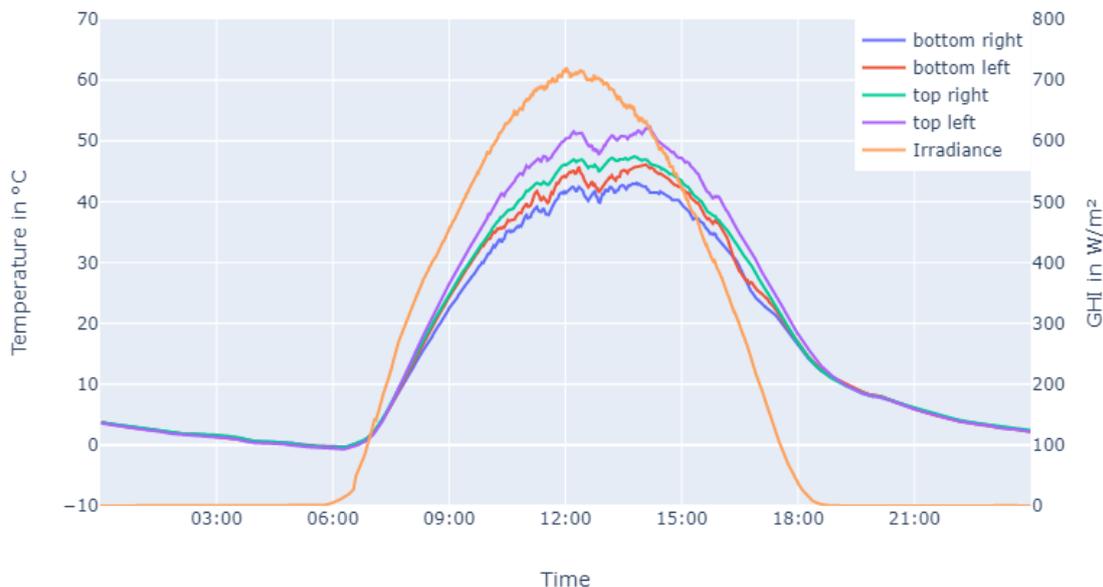
Figure 17: Average string temperature and global tilted irradiance on the 24th of March

This figure shows a steep increase in temperature for each module right after sunrise. As already mentioned in chapter 3.2, the module temperature increases with higher irradiation and higher ambient temperature. This course is clearly visible in Figure 17. Noticeable is the difference between string temperature and irradiance at the peak during noon. While the irradiance clearly shows a stable course without any major fluctuations, the temperature starts to fluctuate at higher values. Therefore, these fluctuations cannot be attributed to the irradiation.

The shape of the temperature curve is slightly more shifted to the afternoon. The effect of thermal inertia can be observed. As expected, the string temperature falls much slower than it rose before.

To visually quantify the influence of the irradiation on the module temperature, a comparison of days with high and low irradiation is necessary. The following Figure 18 shows the same parameters as the previous Figure 17, but on a cloudy day with much less irradiation measured.
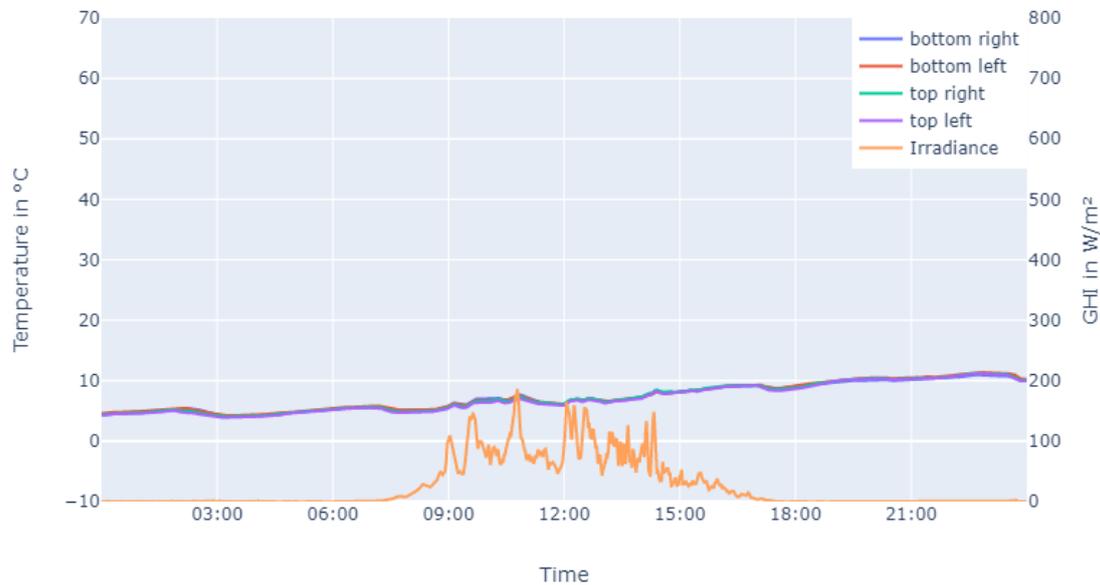

Figure 18: Average string temperature and global tilted irradiance on the 16th of February

In Figure 18 nearly no increase in temperature can be observed. Even though the irradiance has a high fluctuation during daytime, the shown string temperatures do not show any major fluctuations over the course of the whole day. Furthermore, no difference between the different strings in the area under investigation can be observed. This is due to the exceptionally low irradiance during the day. As already shown in Figure 13, on this day nearly no PV power can be generated. Therefore, the PV modules only heat up gradually with the increase in ambient temperature during the day.

Figure 17 and Figure 18 show a clear dependence of the module temperature to the solar irradiation. Only on days with higher module temperatures additional effects on the module temperature can be observed. The cause for the observed fluctuations in Figure 17, is further been investigated in the following chapter 5.3, where the air flow velocity of the rear-ventilation is examined.

5.3 Air flow velocity

As shown in Figure 19, the measured data set of the rear-ventilation shows high fluctuation especially during daytime and high ambient wind speeds. To make an evaluation possible, I smoothen the acquired data.
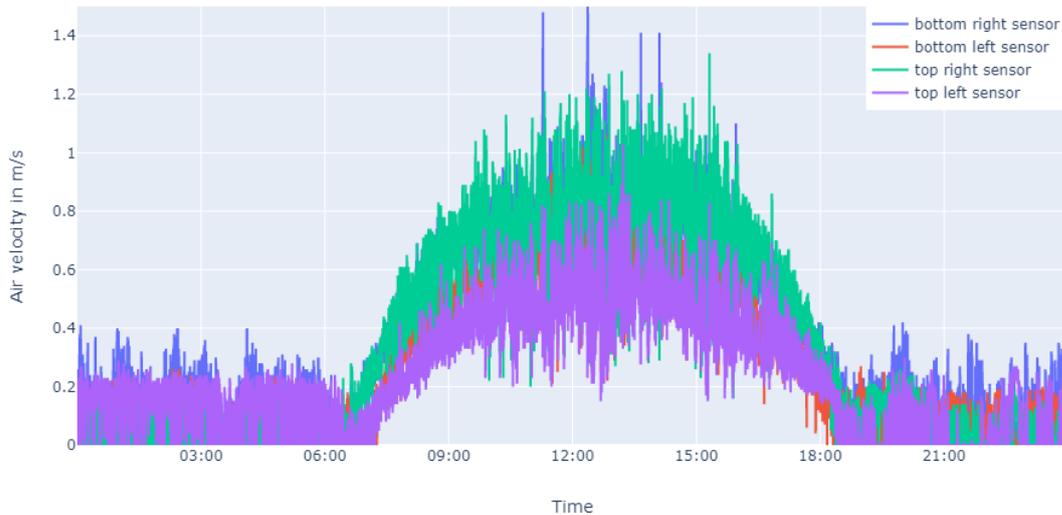

Figure 19: Raw measurement data from the air velocity of the rear-ventilation on the 24th of March

A moving average is applied to smooth out the fluctuations in the air velocity and enhance the comparability. This kind of average is commonly used to eliminate short but high fluctuations on data sets with long-term measurements. With the subset window size of 180 measurements which equals 30 minutes of data the curves get significantly smoother. In the following Figure 20, the average air velocity of the rear-ventilation is shown. Each part of the area under investigation is represented by the color code introduced in Figure 16.
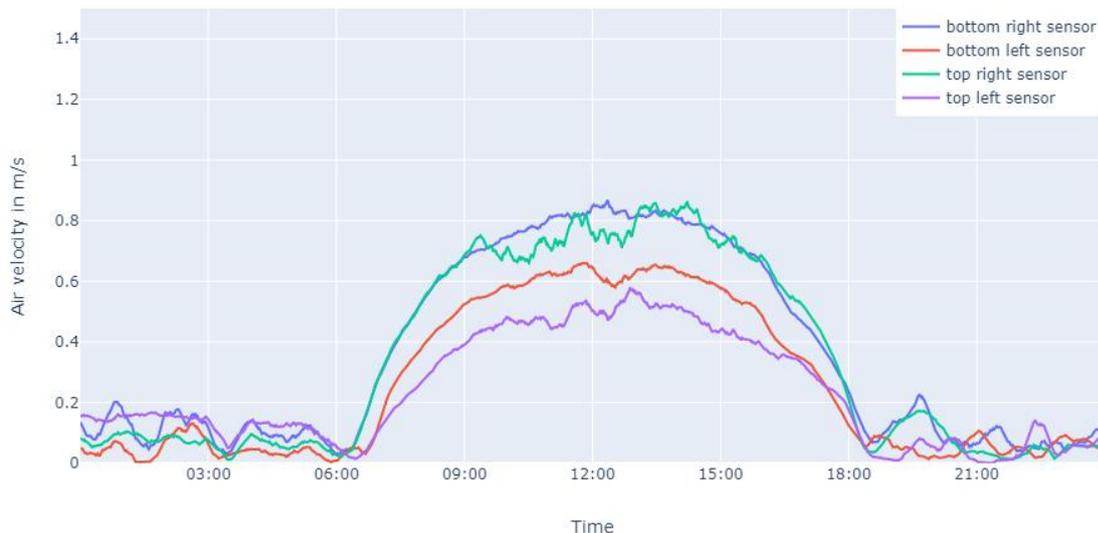
Figure 20: Average air velocity of the rear-ventilation on the 24th of March

During daytime, the air velocity of the rear-ventilation increases. Most noticeable is the difference in air velocity between the smaller and bigger air gap in the area under investigation. All curves show an increase in air velocity at sunrise which peaks at around 12:00 am and then a decrease until sunset to their previous level. All curves are rather similar with only minor differences. The measured data from the right sensors shows a noticeably higher air velocity during the peak around noon. During nighttime almost no air velocity can be measured. Even with the moving average applied a fluctuation is visible.

Since the increase in the rear-ventilation seems to follow the day and night cycle, a further investigation in relation to the irradiance is interesting. In the following Figure 21 shows the same day as in Figure 20 but with the global horizontal irradiance plotted on a secondary y-axis.
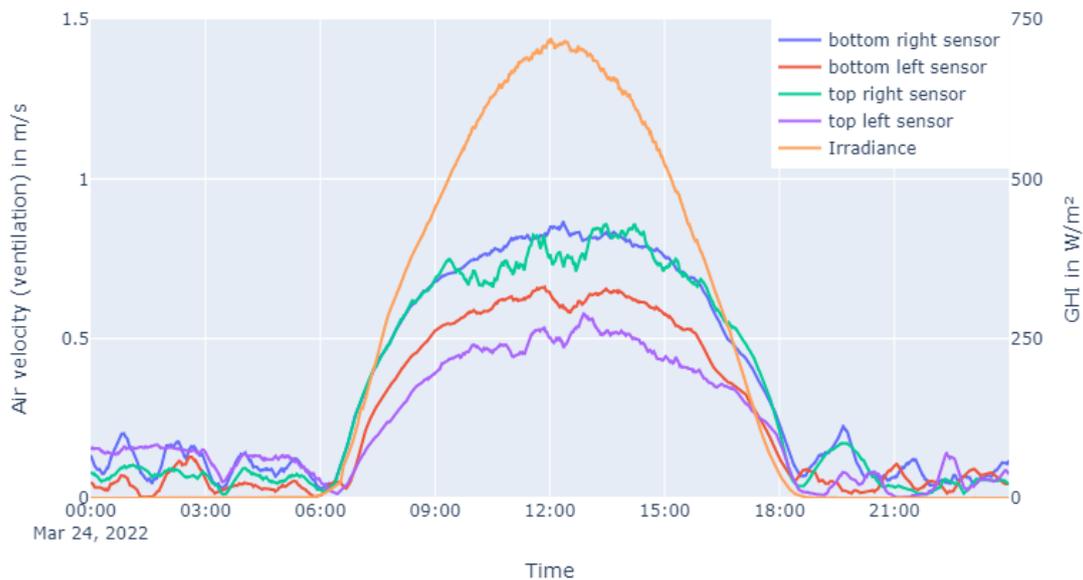

Figure 21: Average air velocity of the rear-ventilation and global horizontal irradiance on the 24th of March

The global tilted irradiance increases simultaneously to the air velocity right as sunrise. The right-side sensors show a much steeper increase in ventilation than the left-side sensors even at low levels of irradiance. Just like the curves for the rear-ventilation, the irradiance peaks during noon and decreases until sunset. The measured course for the irradiance is much smoother than the measured courses for the air velocity of the rear-ventilation. The fluctuation of the air velocity cannot be related to the irradiance. To verify, whether the irradiance is the origin of the measured increase in velocity, a day with less irradiance has to be compared.

Figure 22 shows the same parameters as Figure 21 on a day with much more clouds and therefore much less irradiance. The maximum global horizontal irradiance rarely rises above 100 W/m². A significant fluctuation in the irradiance can also be observed which is caused by the cloud movement.
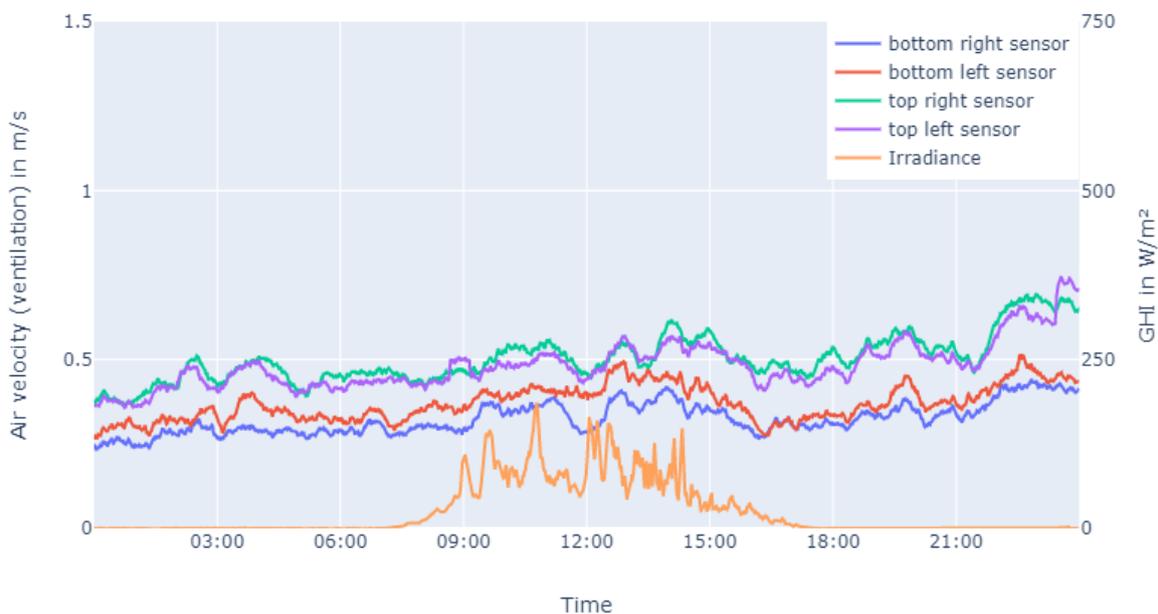
Figure 22: Average air velocity of the rear-ventilation and global horizontal irradiance on the 16th of February

On the cloudy day depicted in Figure 22 no major increase in the air velocity of the rear-ventilation can be measured during daytime. Over the whole day a small but steady increase of around 0.2 m/s can be observed by every sensor. But this overall increase shows no sign of being related to the irradiance because it is also observable during nighttime. Overall, the rear-ventilation seems unaffected by this small amount of irradiance.

Another contributing factor towards the air velocity of the rear-ventilation is the ambient wind speed. Although previous figures seem to show a clear correlation with the irradiance, the shown effect could possibly be a result of high ambient wind speed. Therefore, a comparison of the rear-ventilation and the ambient wind speed is shown in the following Figure 23 and Figure 24.
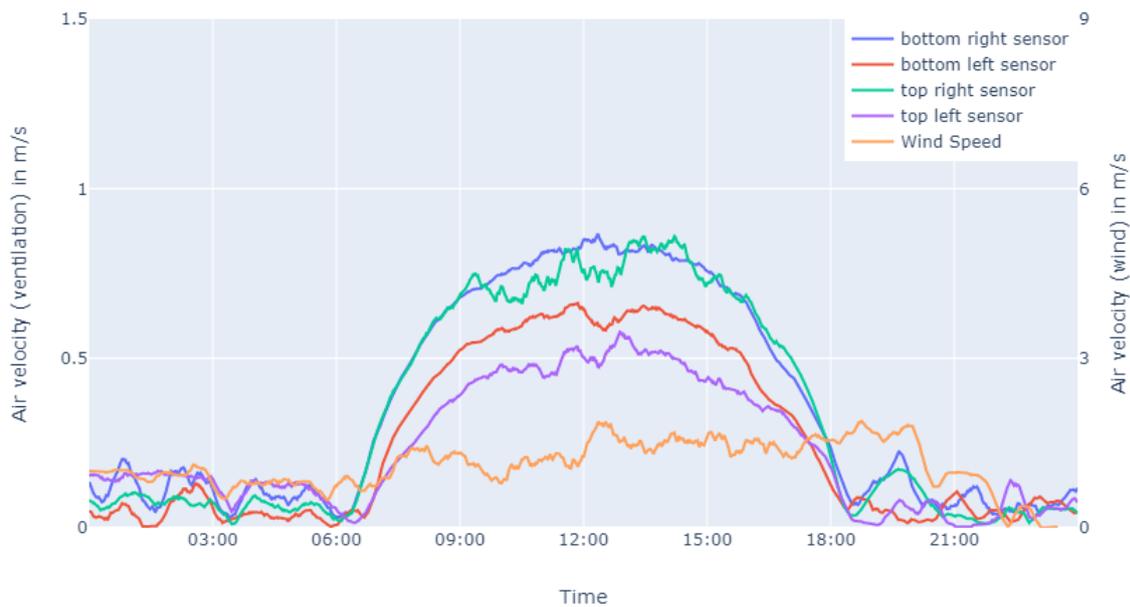

Figure 23: Average air velocity of the rear-ventilation and the ambient wind on the 24th of March

Looking at the 24th of March, no indicator of a correlation between increase of the air velocity of the rear-ventilation and the ambient wind speed can be found. The ambient wind speed shows a fairly stable course over the whole day while the rear-ventilation increases drastically during daytime. Although the ambient wind speed does not cause the major increase in air velocity of the rear-ventilation, it could be the cause of the smaller fluctuations, which even appear at the air velocity peak during noon. The following Figure 24 shows the parameters as the previous figure, but on a day with much less irradiance and much higher ambient wind speeds. Note, that due to the much higher winds speeds, the secondary y-axis in the following Figure 24 and Figure 25 changes in scale in respect to the previous Figure 23.
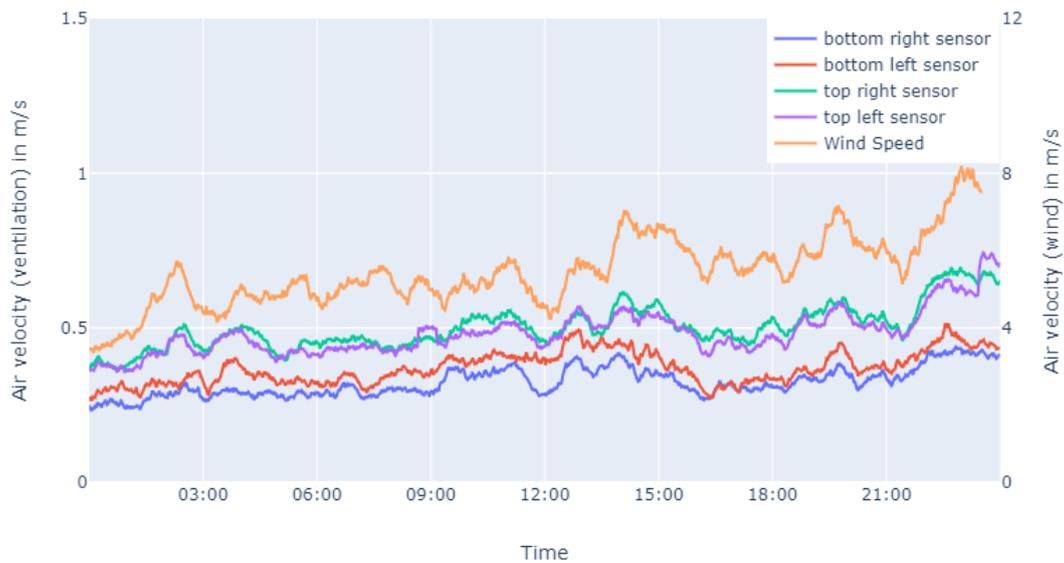
Figure 24: Average air velocity of the rear-ventilation and the ambient wind on the 16th of February

With an up to four times higher ambient wind speed and overall, much higher fluctuations of the wind, a small correlation of the courses can be found occasionally. Some measurement peaks of the ambient wind speed seem to correlate with some smaller fluctuations in the air velocity of the rear-ventilation. The overall stable air velocity of the rear-ventilation takes a similar course than the highly fluctuating ambient wind speed.

In the period under review an extreme weather event took place. Because of record-breaking wind speeds, even Germany's National Meteorological Service (Deutscher Wetterdienst) has labeled this disastrous storm a regional historic natural event [13]. Large parts of west and central Europe suffered from severe storm damages. With measurement during these high wind speeds, the influence on the rear-ventilation is most prominent.
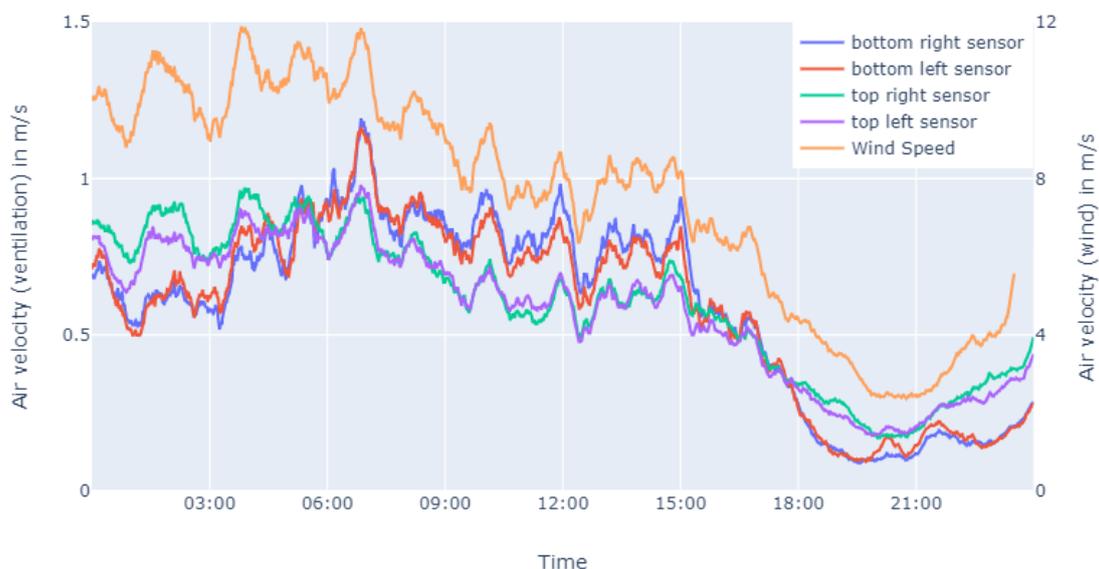
Figure 25: Average air velocity of the rear-ventilation and the ambient wind on the 16th of February

With the uncommonly high wind speeds measured during this extreme weather event an influence on the air velocity of the rear-ventilation can be shown. Positive and negative peaks of the ambient wind speed can also be observed in the air velocity of the rear-ventilation. A correlation of the wind speed and the air velocity of the rear-ventilation can therefore be proven. Even though the influence decreases with a lower wind speed, the fluctuations in the air velocity of the rear-ventilation are at least partly caused be the ambient wind speed.

5.4   Influence on the PV power output

The following Figure 26 shows the data sets of every single exemplary measurement during one selected day. The figure shows the measurements of the area under investigation on a day with high solar irradiation and an overall high performance of the PV system.

The top part shows the difference in the PV power output between the smaller and bigger air gap from the area under investigation. Additionally, the global tilted irradiance is shown for reference. The middle part shows the module rear temperature, from which the average rear temperature for the whole string has been formed. For this part, the ambient temperature is shown as reference. In the bottom part, the average air velocity of the rear-ventilation is depicted. Here, the average of the ambient wind speed serves as reference.

Most noticeable is the fact that even though differences in temperature and ventilation can be observed, nearly no differences in PV power can be spotted at first glance.
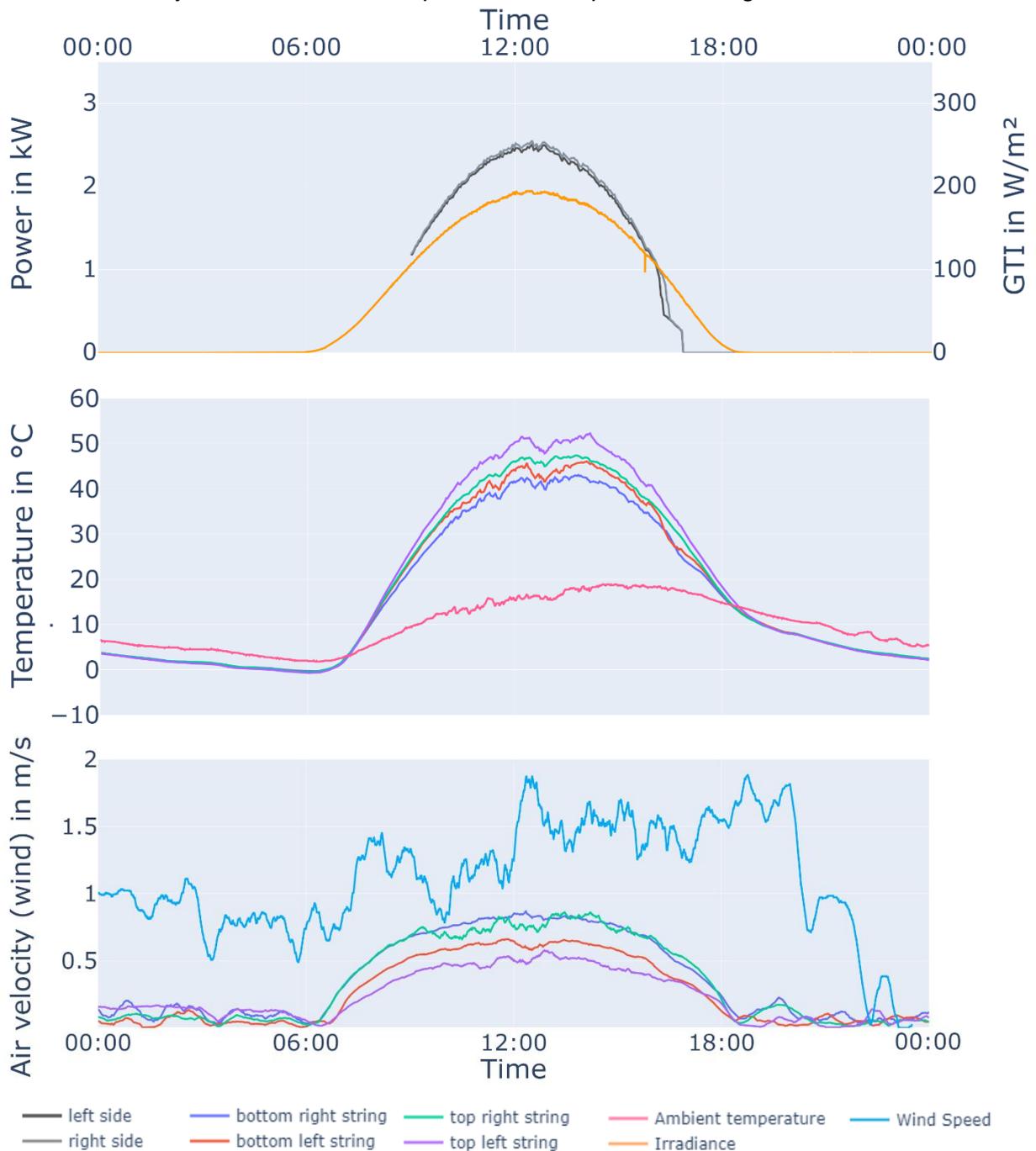

Figure 26: Overview over every measurement on the 24th of March

6 Results

6.1 Difference in rear-ventilation

The measurement of the air velocity of the rear-ventilation shows a high difference between both facade substructure variations. While the sensors on the right side with the bigger air gap measure a much higher air velocity than the sensors on the left side, the course of the measurements from both sensors are in a similar shape.

Usually, small to non-observable rear-ventilation can be measured during nighttime and if so, fluctuations can be observed. These fluctuations still can be observed during daytime, but mostly with less amplitude. The air velocity increases and decreases with the intensity of the solar irradiation as shown in chapter 5.3. High ambient wind speeds can also have a major impact on the rear-ventilation, but the occurrence during the measurement period is seen as an exception.
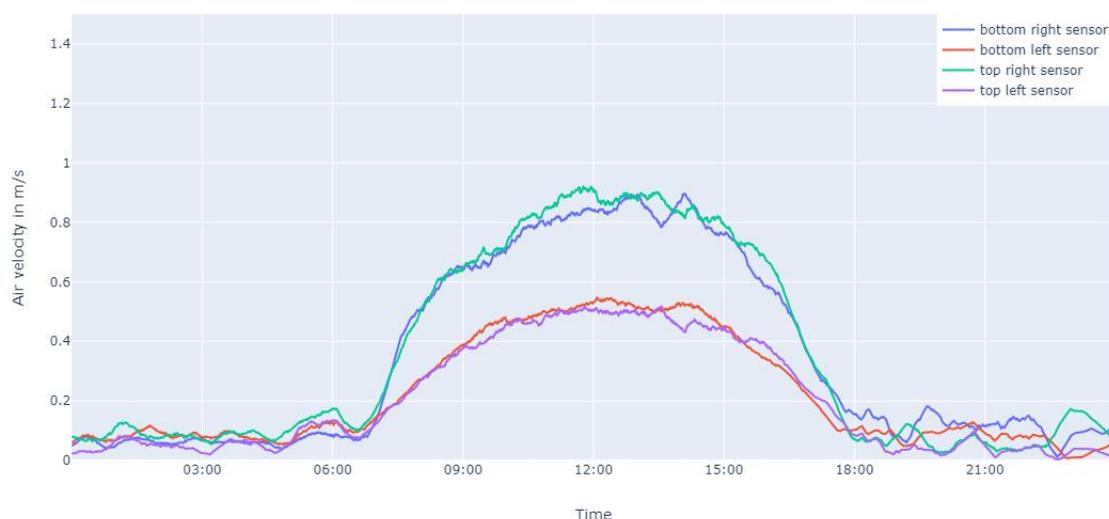

Figure 27: Average air velocity of the rear-ventilation on the 1ˢᵗ of March

The difference, which is shown in Figure 27, cannot be fully explained by the other measured parameters such as the module rear temperature. The reason could hypothetically be the smaller air gap, which possibly restricts the air flow. Even though the air gap is bigger than recommended minimal size of 2 cm for standard ventilated curtain wall facades without PV modules [14], proper air flow cannot be guaranteed. The module substructure, cables and measurement sensors could lead to a higher friction and therefore to a decrease in the air velocity. Additionally, some of the insulation mats could narrow down the air gap.

Thorough documentation of the construction process revealed that some of the insulation mats had protruding corners and edges. These can also be spotted in **Fehler! Verweisquelle konnte nicht gefunden werden.** and **Fehler! Verweisquelle konnte nicht gefunden werden.**. In addition, it cannot be guaranteed that the air gap is not completely blocked at individual points behind the modules. It must be assumed that irregularities in the size of the air gap were created, which are difficult to reconstruct after the installation of the PV system. The influence of these irregularities is much higher for the air gap on the left side because an unwanted narrowing could quickly lead to an undersized air gap without proper air flow.

6.2   Difference in module temperature

The investigation of the module rear temperature not only shows a difference between the sensors at the smaller and bigger a gap, but also a difference between the top and bottom sensors. The differences in temperature are much smaller than the air velocity differences in the rear-ventilation. As depicted in Figure 28, the upper module strings have a higher temperature than the lower ones. Furthermore, both left strings have a higher temperature than both right strings.
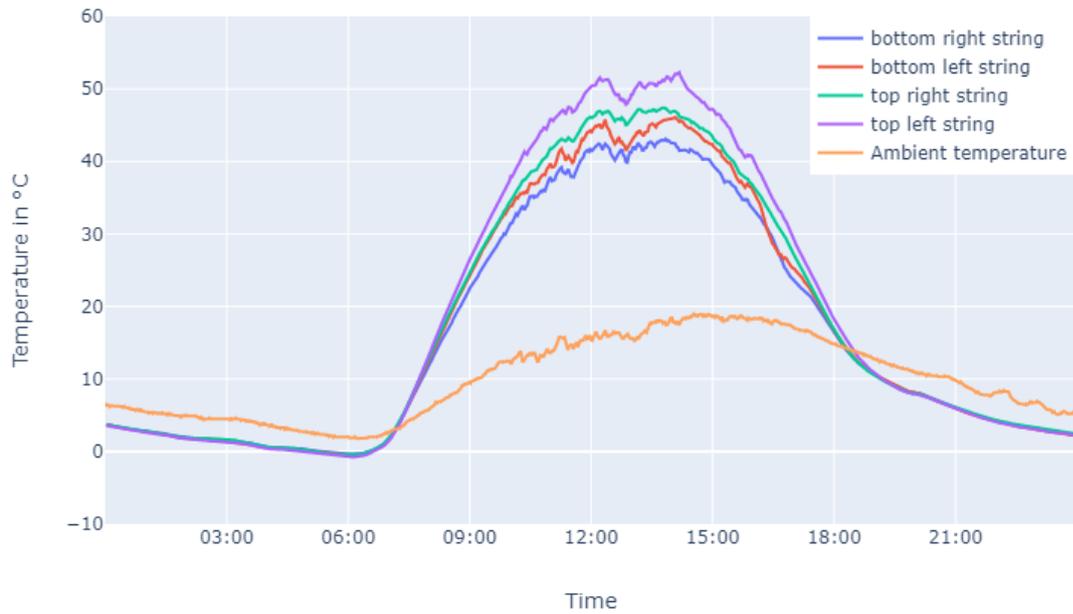

Figure 28: Average string temperature in contrast to the ambient temperature on the 24th of March

As expected, the module rear temperature increases with the rising of the sun and the associated increase in solar irradiation. As stated in chapter 5.2, the fluctuations during the temperature peak in Figure 28 are a result from the cooling of the ambient wind and the rear-ventilation since the global tilted irradiation doesn't show any fluctuation during this day.

During nighttime no major fluctuations of the temperature can be observed. The course follows steadily the course of the ambient temperature with a small discrepancy. This is perfectly normal behavior for metal objects because of their high thermal conductivity.

The minor difference in the module rear temperature between the left and right side is a result of the major difference in the air velocity of the rear-ventilation. On the right side of the area under investigation the higher air velocity of the rear-ventilation leads to an overall lower module temperature. The left side with the noticeable lower air velocity of the rear-ventilation therefore shows the overall higher module temperature.

The temperature difference between the upper and lower strings is an effect of the usual heat transfer behavior of a heat exchanger. Less heat flow on the top of the facade leads to less cooling of the solar modules. On the lower facade, the temperature difference between the solar modules and the air is higher, which is why more heat can be transferred to the air. This difference increases with greater building height. On a smaller building this effect wouldn't be as clearly visible in the measurements.

6.3 Difference in PV power output

In contrast to the obvious differences in the module temperature and rear-ventilation, the difference in the PV power output is not as clear. During an overall sunny day without clouds and therefore high and barely fluctuating solar irradiation, differences can only be spotted in the afternoon.

Figure 29 shows such a day on the 1st of March, where starting at 2:30 p.m. the power on the left side of the area under investigation drops. An hour later fluctuations take place while both courses have converged again. By looking closely at the power peak, a small difference between both sides can be observed. The left side seems to generate slightly less power than the right side. This minor difference will be later discussed and weighted for significance.
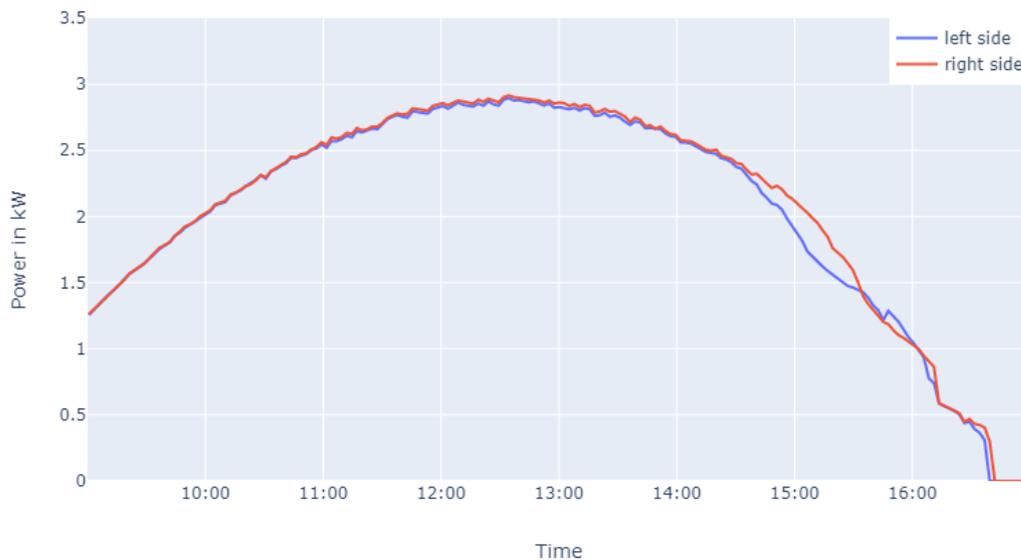

Figure 29: PV power from two different facade substructure variations on the 1st of March

The major difference in power on the afternoon can be spotted on several days and most prominent is this difference during winter. In chapter 5.1 this difference in the afternoon is attributed to a shading problem. A tree is casting a shadow which moves over the course of a couple of hours over the lowest modules on the facade. Figure 30 shows such a winter day, where these shading problems are much higher than during March. The shadow is moving from the left to the right side and thus creates two courses which show a helix like shape.
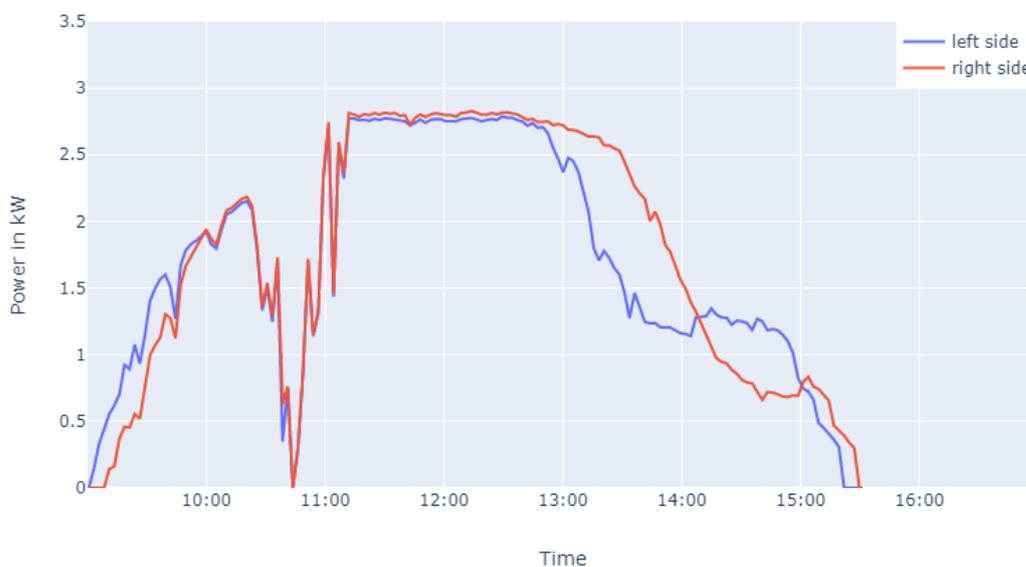
Figure 30: PV power from two different facade substructure variations on the 25th of December

During winter, this loss in power can also be spotted in the morning hours. The right side of the area under investigation generates a much lower power output than the left side. This is also due to a shading problem, which is caused by the low angle of the sun and resulting shadows from nearby vegetation. On this particular day, between 10:00 and 11:00 a.m., a major drop in power can be observed which is a result of a sudden decrease in irradiation. This decrease is not caused by a shadow from the vegetation, but rather by cloud movement. An indicator for the difference between a cloud shadow or a vegetation shadow is the comparison of the difference in PV power output between both facade substructures. If a high difference between both curves can be observed, the shadow is most likely caused by vegetation. If a low difference or none at all is observed, the shadow is most likely caused by cloud movement. Therefore, the exceptionally high differences in the PV power output between both facade substructures should be put aside for the evaluation, which facade substructure performs better.

To conclude how often major or minor differences in the PV power occur, the following Figure 31 compares them to the total number of measurements over the course of three months starting at the 2nd of January. A high count in percent shows, that the depicted absolute difference in power has a high occurrence in the period under review. Note, that measurements only took place during daytime. The similarity during nighttime has not been included in the following figure, to assure a proper comparison only during operational hours.
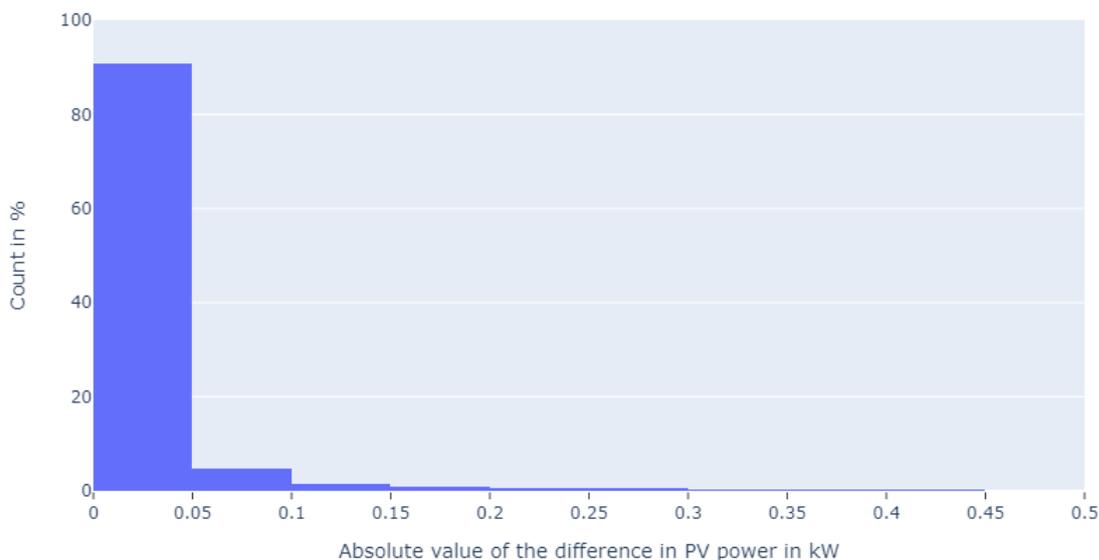

Figure 31: Absolute difference in PV power from two different facade substructure variations (02.01. – 02.04.2022)

Most noticeable is the exceptionally high count in small differences. 90,7 % of all measured differences in the generated power of both facade variations show an absolute value of 0 to 0,05 kW. 4,6 % of all measured values show a slightly higher absolute difference from 0,05 to 0,1 kW difference. The remaining 4,7% of all measured values spread over the rest of the depicted bins. All absolute differences lie within the range of 0 to 0,5 kW, except individual outliers, which haven't been included in the final figure.

Higher absolute values of the difference in the generate PV power only occur rarely. Since the period under review for Figure 31 starts on the 2nd of January, most days with a particularly low sun angle have already passed. High differences in power due to the shading problems were still expected but did not occur as often as during the December.

Since over 95 % of all measured absolute values lie within the range of 0 to 150 W difference of the generated PV power output, further investigation of this section has been done. Looking at the plain difference in the PV power between both facade substructures, a statement can be made, whether one of both module areas performs better. The following Figure 32 the difference in generated PV power from both facade substructure variations
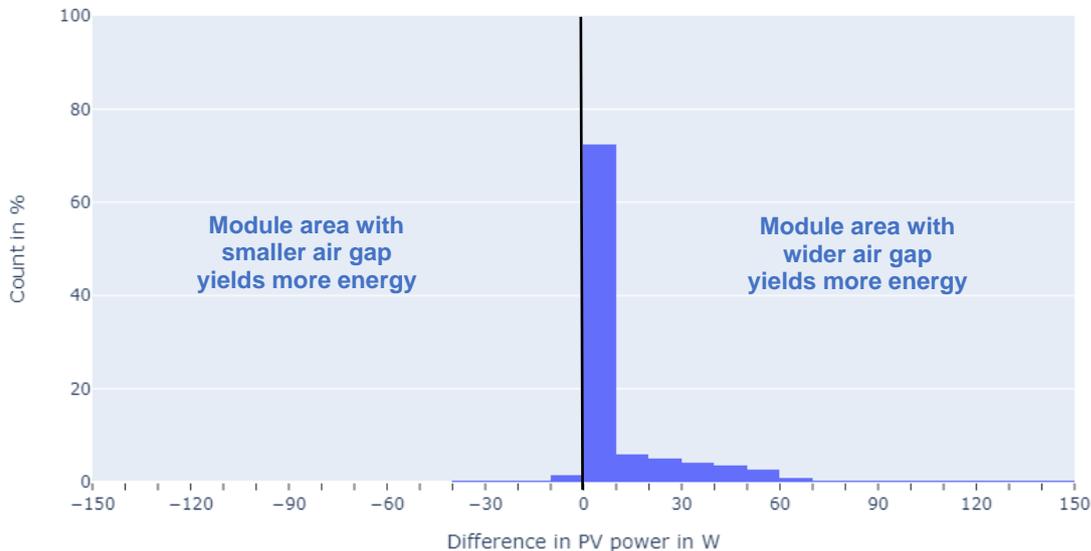
Figure 32: Difference in PV power from two different facade substructure variations (02.01. – 02.04.2022)

A clear shift towards the right side can be observed in this figure. Most of the measured differences in power are still in the smallest bin on the right side, although it has shrunken in size down to 72,3 %. Since all bins are clearly divided by positive and negative values, nearly all smaller differences have now been attributed to a higher power from the module area of the substructure with the wider air gap. Apart from the exceptionally high bin, the other bins on the right side all show a difference in power, which cannot be attributed to measurement uncertainties.

The PV modules of the facade substructure with the smaller air gap get consistently outperformed by the other modules. Even though the difference in the generated power is usually respectively small, it adds up over time. If the generated power of both variation is put into relation, the amount of generated power over time was around 1,65 % higher on the right side with the wider air gap. This seems to prove, that the facade substructure with the wider air gap has a beneficial effect on the performance of the generated PV power.

Although this assumption is not fully incorrect, a main contributing factor has been overlooked. As shown in Figure 29, fluctuations due to shading problems still can be observed in the early months of spring. A major part of the total difference in power still is caused by shading. Because the group of trees is located in the South-West of the area under investigation, the module area with the smaller air gap can still be shaded, when the shadow is too short to reach the area with the wider air gap.

However, Figure 31 also shows a difference between both variations during noon, where no shading from a nearby obstacle could influence the generated PV power. If the measurements during this small period are set into relation, a much smaller lead of 0,78 % for the right side can be calculated. Regarding the calculated average relative error for the generated PV power of 0,212 %, which has to be applied to both sides, this difference can be labeled insignificant.

7   Conclusion

This study shows that for the investigated building a variation of the air gap and the insulation thickness in the facade substructure has barely an influence on the PV performance during the time of observation. Compared to the total power of the considered area, the measurable difference between a smaller air gap (5 cm) with a thicker insulation and a bigger air gap (15 cm) with a thinner insulation must be labeled as insignificant.

The investigation of the air velocity of the rear-ventilation shows major differences, which only have a minor influence on the module temperature yet. The side of the area under investigation with the bigger air gap shows a much higher air velocity, which contributes to a better cooling of the modules. The smaller air gap on the left side partially restricts the air flow of the rear-ventilation due to the various electrical components located inside the air gap and an unclean installation of the insulation mats.

Further investigation of the rear module temperature showed only small differences between the monitored strings. Higher located module strings show a higher temperature than lower ones. The upwards moving air heats up and therefore, a lower heat transfer is possible. The better ventilation on the right side of the area under investigation results in a smaller increase in module temperature during operation.

The observed differences in the generated PV power had a different origin as first expected. A group of nearby trees caused shadowing and thus a substantial difference in the generated power between both investigated substructure variations. The loss in power due to the shading was particularly high during December because of the respectively low angle of the sun. The effects of this problem decreased continuously over time. It is to be expected that no influence will be recorded during summer months due to the higher angle of the sun.

Nevertheless, during the period under review it was impossible to compare the PV power output over a longer period without including the influence of shading. While looking at a selected day without any shading at noon, then a minor difference of 0,7 % can be observed. The right facade substructure variation with the bigger air gap consistently generates a tiny amount more power than the left facade substructure variation with the smaller air gap. Considering the applied relative error of around 0,2 %, this difference has been rendered insignificant. I recommend checking the incoming data from this installation again after a full year of data acquisition, since changing temperature conditions and different shading situations will highly influence the generated PV power. This lies beyond the scope of this work and will be subject to further research.

How can this knowledge help us in the future?

Architects and planners need freedom in the process of designing and planning of a building. The complex element "PV module" has many requirements for usage and limited aesthetic variety. For that reason, BIPV is not as common in newly constructed buildings as it could be. Every requirement or limitation, which can be eliminated, simplifies the usage of these products. More and more BIPV systems will be constructed, because the whole designing and planning process can be slowly facilitated.

Architects don't have to worry about the size of air gaps in ventilated curtain wall facades made of PV modules. They can use the optimal air gap to ensure moisture drainage without accidentally restricting the PV system from power generation. This being said, the integrated PV module is similar to any other building element in respect to its integration in building facades.

8   List of references

[1] S. H. M. H. Michael Koehl, „Effect of thermal insulation on the back side of PV modules on the module temperature,“ *PROGRESS IN PHOTOVOLTAICS: RESEARCH AND APPLICATIONS,* 2016.

[2] J.-B. Eggers, M. Behnisch, J. Eisenlohr und H. Poglitsch, „PV-Ausbauerfordernisse versus Gebäudepotenzial: Ergebnis einer gebäudescharfen Analyse für ganz Deutschland,“ in *35. PV-Symposium*, Bad Staffelstein, 2020.

[3] (ed.), DIN German Institute for Standardization, Photovoltaics in buildings - Part 1: BIPV modules; German version EN 50583-1:2016, Beuth Verlag GmbH, VDE Verlag GmbH, 2016.

[4] (ed.), Consulting office for building-integrated Photovoltaics, „BIPV? What's this?,“ Helmholtz-Zentrum Berlin für Materialien und Energie GmbH, [Online]. Available: https://www.helmholtz-berlin.de/projects/baip/bipv_en.html. [Accessed on 07.04.2020].

[5] V. Quaschning, Understanding Renewable Energy Systems, Bd. Second Edition, London: Earthscan from Routledge, 2016.

[6] L. Maturi, G. Belluardo, D. Moser und M. Del Buono, „BiPV system performance and efficiency drops: overview on PV module temperature conditions of different module types,“ *ScienceDirect,* September 2013.

[7] P. Kosky, R. T. Balmer, W. D. Keat und G. Wise, „Chapter 14 - Mechanical Engineering,“ in *Exploring Engineering: An Introduction to Engineering and Design*, Elsevier Inc., 2021.

[8] L. Laloui und A. F. Rotta Loria, „Chapter 3 - Heat and mass transfers in the context of energy geostructures,“ in *Analysis and Design of Energy Geostructures*, Elsevier Inc., 2019.

[9] W. Lichten, Data and Error Analysis in the Introductory Physics Laboratory, Boston: Prentice Hall College Div, 1988.

[10] P. Profos und T. Pfeifer, Grundlagen der Meßtechnik, Bd. 5. Auflage, München; Wien;: R. Oldenbourg Verlag, 1997.

[11] H. Hart, Einführung in die Meßtechnik, 5., durchgesehene Auflage, Berlin: VEB Verlag Technik Berlin, 1989.

[12] ISO 9060:2018, Solar energy - Specification and classification of instruments for measuring hemispherical solar and direct solar radiation, 2018.

[13] Deutscher Wetterdienst, „Orkan ZEYNEP - Ein regional historisches Naturereignis,“ 19 02 2022. Available: https://www.dwd.de/DE/wetter/thema_des_tages/2022/2/19.html. [Accessed on 09.04.2022].

[14] Fachverband Baustoffe und Bauteile für vorgehängt hinterlüftete Fassaden e.V. (FVHF), „Planning and Constructing Rear Ventilated Rainscreen Facades - FVHF Guideline,“ 01 03 2018. [Online]. Available: https://www.fvhf.de/Fassade-bilder/docs/FVHF-Guideline_ Planning-and-Constructing-Rear-Ventilated-Rainscreen-Fac-ades_180306_EN.pdf. [Accessed on 13.04.2022].

9   Appendix

**Figure 33: Group of trees (left) casting shadows on the area under investigation (right)**
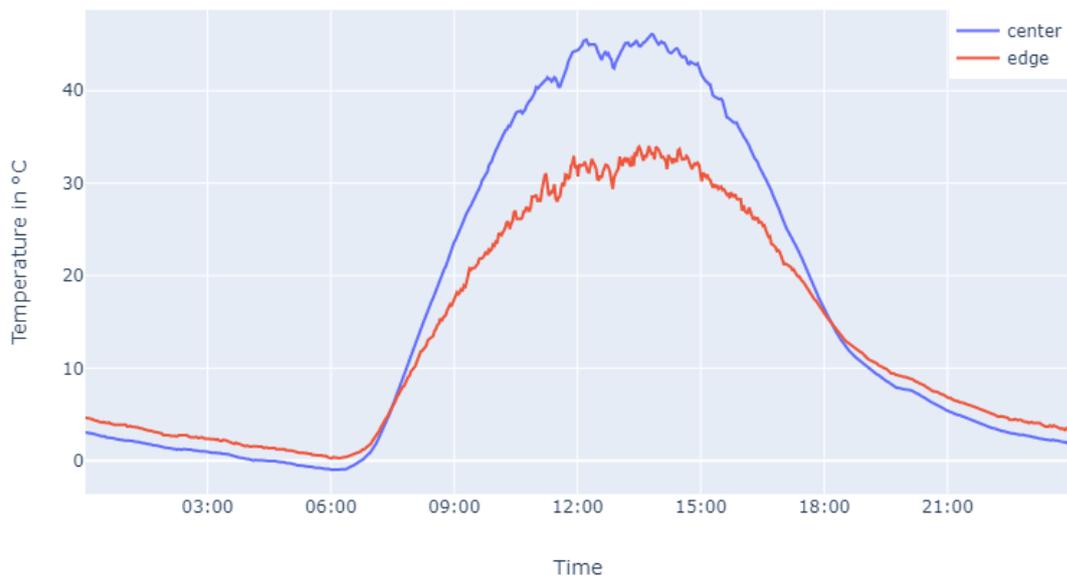
Figure 34: Single defective sensor for the edge module temperature measured at a selected PV module at the bottom on the 24th of March

10 Statement of independent work

I hereby declare that

- I have done this scientific work independently and without any unauthorized assistance,
- I have not used any sources and materials other than those indicated,
- I have marked the passages taken from the sources used as such,
- the work in the same or similar form has not been submitted to any other audit authority

Berlin, 14th of April 2022